Hindawi
Geofluids
Volume 2021, Article ID 5392976, 15 pages
https://doi.org/10.1155/2021/5392976

Research Article

Analysis of Soil Resistance under Horizontal Load of Rigid Antislide Pile

Zhenyu Song,[1] **Yuanyuan Kong**,[1] **Siqi Wang**,[1] **Weifeng Zhao**,[1] **Lu Chen**,[1] **and Kai Feng**[2]

[1]*Chang'an University, College of Highway, Xi'an, Shanxi Province, China*
[2]*Chongqing University, School of Civil Engineering, Shapingba, Chongqing 400044, China*

Correspondence should be addressed to Yuanyuan Kong; kongyy@chd.edu.cn

Received 8 July 2021; Revised 6 September 2021; Accepted 18 September 2021; Published 8 October 2021

Academic Editor: José Luis Pastor

In order to study the bearing characteristics and failure mechanism of the rigid antislide pile under horizontal load, the stress of rigid antislide pile under transverse axial large displacement load is analyzed by using elastic-plastic theory, finite element analysis, and model test. The theoretical formula of the proximal plastic earth pressure near the pile with the depth of soil under the horizontal force is obtained. The results show that the standard is insensitive to the variation of soil parameters and the influence of soil parameters on allowable soil resistance in front of pile should be considered. With the increase of the horizontal force of the pile top, the soil near the pile is destroyed in this process gradually, which is the decline of the cross section of the maximum soil resistance of the pile. When the horizontal displacement of pile top is 20 mm and 70 mm, the soil resistance value and the ultimate soil resistance value in front of the pile can be selected, respectively. The plastic zone develops to the front and bottom of the pile at the same speed, at an angle of 45° with the direction of gravity. When the displacement reaches 34 mm, the plastic zone develops to the deeper depth obviously. The results can provide a theoretical basis for the design and application of antislide piles during the process of slope protections.

1. Introduction

There are lots of rocky slopes or steep terrain during road construction. The rock and soil body of the slope is prone to instability and landslide and then affects the construction and normal operation of the highway when it is affected by hydraulic action, earthquake, artificial blasting, and other factors. Antislide pile plays an indispensable role in the protection of slope engineering among many slope treatment schemes.

The main function of an antislide pile is to resist sliding thrust from soil to maintain slope stability. To maintain such a steady state, the antislide pile shall first produce sufficient resistance to the surrounding soil and shall not be broken or produce large tilt and displacement [1]. Accordingly, it is necessary to solve the analytical formula under the joint action of the eccentric load on the pile top and the horizontal distributed load on the pile body [2] and to find out the landslide thrust acting on the antislide pile and the transfer relationship between the antislide pile and the forward sliding force of the pile [3]. In theory, Xiao [4] established the mechanical analysis model of H-type antislide pile and achieved good practical results; Zhang et al. [5] considered the response of foundation reaction coefficient to horizontal pile under load; Yokoyama [6] systematically summarized various calculation methods of pile lateral resistance. As for the calculation of internal force and soil resistance of horizontal load pile, the p - y curve method is one of the most widely used methods in the world. It takes into account the nonlinear and stratified characteristics of soil and is suitable for large horizontal displacement of pile top due to horizontal axial load of pile [7]. Matlock [8] proposed the p-y curve method combining the results of indoor soil triaxial compression test with stress-strain when studying the resistance law of soil at the side of the pile under lateral load. Subsequently, the p-y curve pile foundation stress calculation

method [9, 10] of soft clay and sand was also established through dynamic and static load tests. For example, Wang et al. [11] studied the performance of piles under lateral static load test and single, two-way cyclic load test. Wang et al. [12] analyzed the influence of clay strength parameters on the *p-y* curve and proposed the calculation method of the *p-y* curve of silt through indoor model test. Later, researchers [13, 14] took the influence of seismic liquefaction, saturation, and change of excess pore pressure in weakened sand on the calculation of the *p-y* curve into account. At the same time, some scholars studied the soil arching effect generated by antislide pile in simulated landslide [15] and the damage mechanism of the interaction between micro-antislide pile and soil [16] through the finite difference method and then compared with the results of model tests [17, 18] and put them into practice, both of which achieved good engineering benefits.

On the basis of the above research results, the elastic-plastic theory was firstly analyzed in this paper; the corresponding formula for calculating the resistance of plastic soil in the horizontal direction of pile foundation is established, which was compared with the current standard document. The resistance behavior of soil in front of rigid antislide pile under large displacement load in horizontal direction was analyzed by using finite element software. Then, it was compared with the indoor model test. The purpose of this paper is to solve problems such as the lack of theory of pile ultimate bearing capacity, the incomplete calculation method in the relevant fields, and to provide technical indexes and theoretical basis for the design of soil resistance in front of rigid antisliding piles.

2. Theoretical Analysis of Ultimate Soil Resistance in Horizontal Direction

2.1. Calculation of Plastic Load under Uniform Strip Load

2.1.1. Calculation of a Point Stress in Soil. Assuming that the soil in question is a semi-infinite elastomer and the soil surface acts on the uniform load p. At this point, the relationship between the maximum and minimum principal stresses σ_1 and σ_3 at any point Q in the soil is as follows:

$$\left.\begin{matrix}\sigma_1\\ \sigma_3\end{matrix}\right\} = \frac{\sigma_1+\sigma_2}{2} \pm \sqrt{\left(\frac{\sigma_x+\sigma_2}{2}\right)^2 + \tau_{xz}{}^2}, \tag{1}$$

$$\tan 2\theta = \frac{2_{xz}}{\sigma_x - \sigma_z}, \tag{2}$$

where θ is the angle between the direction of action of σ_1 and the vertical direction.

According to Boussinesq's solution, when the foundation has no buried depth, the relationship between principal stresses is as follows:

$$\left.\begin{matrix}\sigma_1\\ \sigma_{13}\end{matrix}\right\} = \frac{P}{\pi}(2\alpha \pm \sin\alpha). \tag{3}$$

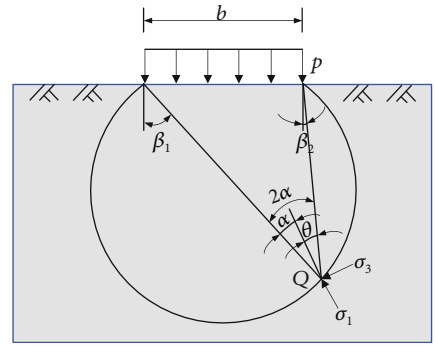

Figure 1: The isogram of principal stress under uniform strip load.

It can be seen from Equation (3) that there is only one variable in the equation, α. Therefore, under the premise of the two points of viewing angle being the same, the principal stress is also the same. In other words, points with equal principal stresses in the soil can be enclosed into a circle with the width of uniformly distributed load b as the chord length and 2α as the circumferential angle, as shown in Figure 1.

2.1.2. Determination of Plastic Zone Range. The additional stress acting on the base surface is $p - \gamma_0 D$, D is the embedded depth of the foundation, p is the total stress of the base surface under the action of external load, and $\gamma_0 D$ is the dead weight stress at the base.

Under the premise of equal self-weight stress of soil (lateral coefficient of soil $K_0 = 1$), the compressive stress of soil self-weight in all directions is $\gamma_0 D + \gamma Z$. Then, the principal stress of any point Q in the soil under the action of total stress can be obtained when the foundation has buried depth:

$$\left.\begin{matrix}\sigma_1\\ \sigma_3\end{matrix}\right\} = \frac{p-\gamma_0 D}{\pi}(2\alpha \pm \sin 2\alpha) + \gamma_0 D + \gamma Z, \tag{4}$$

where γ_0 is the weighted average weight of the soil above the basement and γ is the weight of the soil below the basement.

When point Q is in the ultimate state of shear failure, its principal stress satisfies

$$\sin\varphi = \frac{1/2(\sigma_1 - \sigma_3)}{1/2(\sigma_1 + \sigma_3) + c\cdot\cot\varphi}. \tag{5}$$

Equations (4) and (5) are solved simultaneously, and after sorting out, we can get

$$Z = \frac{p-\gamma_0 D}{\gamma\pi}\left(\frac{\sin 2\alpha}{\sin\varphi} - 2\alpha\right) - \frac{c\cdot\cot\varphi}{\gamma} - \frac{\gamma_0}{\gamma}D. \tag{6}$$

The above formula is the extended depth of plastic zone under horizontal load of pile top. Under the condition of known uniform load p, action width b and α, and various strength parameters of soil, the depth Z can be obtained,

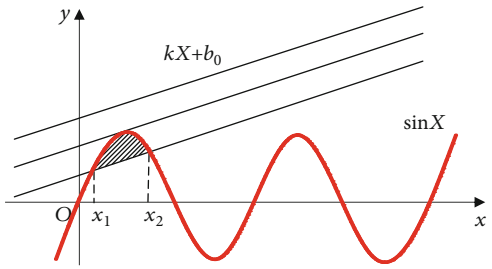

Figure 2: Curve relation of critical state equation.

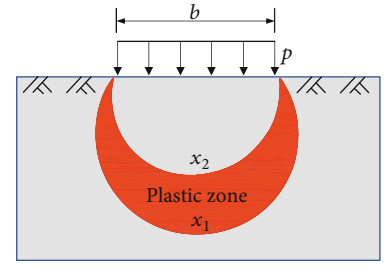

Figure 3: Plastic region.

and the points of different depths Z can be connected to obtain the extended range of plastic zone in soil.

2.2. Calculation of Resistance of Plastic Soil in Horizontal Direction in front of Pile. Based on the assumption of Winkler foundation model and the solutions of large and small principal stresses under infinite uniform strip load, the critical soil resistance at the pile side can be calculated. The principal stress expression of any point Q in the soil in front of the pile under horizontal load is obtained. Here, $p - \gamma_0 D$ is replaced by σ_h, $\gamma_0 D + \gamma Z$ is replaced by $\gamma h k_0$, and k_0 is the static earth pressure coefficient, as shown in

$$\left.\begin{matrix}\sigma_1\\ \sigma_3\end{matrix}\right\} = \frac{\sigma_h}{\pi}(2\alpha \pm \sin 2\alpha) + \gamma h k_0. \tag{7}$$

The principal stress at a certain point in the soil layer and the soil strength parameters must satisfy the inequality relationship as shown in Equation (8), if the stress state is tangent to or intersects the strength envelope, according to the Mohr-Coulomb strength theory.

$$\frac{\sigma_1 - \sigma_3}{2} \geq \left(\frac{\sigma_1 + \sigma_3}{2} + \frac{c}{\tan\varphi}\right)\sin\varphi. \tag{8}$$

Here, when we set $b_0 = (\pi/\sigma_h)(\gamma h k_0 \sin\varphi + c\cos\varphi)$, $X = 2\alpha$, and $k = \sin\varphi$, Equation (8) also can be simplified as

$$\sin X \geq kX + b_0. \tag{9}$$

In this way, the above problem can be simplified to the position relationship between $\sin x$ and $kx + b_0$ as shown in Figure 2. At intersection of Figure 2, the stress state at this point changes from elastic to plastic, and x_1 and x_2 are the upper and lower boundaries of the plastic zone as shown in Figure 3.

According to the relationship between the critical state, Equation (9) can be solved to obtain the relationship between soil resistance σ_h in front of the pile and depth h:

$$\sigma_h = \pi\frac{\gamma h k_0 \sin\varphi + c\cos\varphi}{\cos\varphi - ((\pi/2) + \varphi)\sin\varphi}. \tag{10}$$

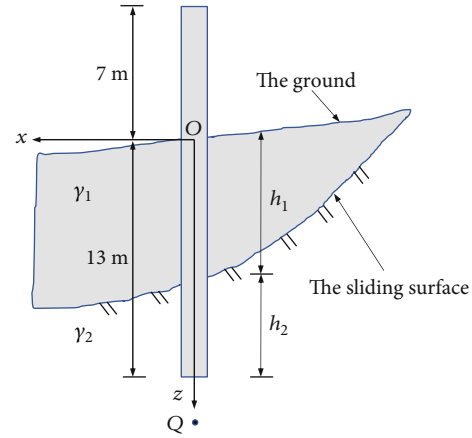

Figure 4: Diagram of buried depth of pile.

As the compressive gravity stress $\gamma h k_0$ exists in all directions, the resistance of the plastic soil in front of the pile is calculated as follows:

$$\sigma_H = \pi\frac{\gamma h k_0 \sin\varphi + c\cos\varphi}{\cos\varphi - ((\pi/2) + \varphi)\sin\varphi} + \gamma h k_0. \tag{11}$$

Under the condition of known soil parameters, formula (10) can be used to obtain the theoretical formula of resistance of plastic soil in front of pile with soil depth Z.

3. Theoretical Analysis and Specification Comparison

In order to facilitate the calculation, the comprehensive internal friction angle ϕ_0 is usually adopted to replace the shear strength c and φ of soil within the influence range of pile [18], and its value can be calculated according to Equation (11), according to the principle of equal shear strength.

$$\phi_0 = \arctan\left(\tan\varphi + \frac{2c}{\gamma H}\right), \tag{12}$$

where H is the soil penetration depth of pile.

In order to satisfy the requirement that the horizontal compressive stress should not exceed the horizontal allowable soil resistance of the foundation (refer to the provisions on the design load and calculation of antisliding

Table 1: Calculation parameters.

Poisson's ratio μ	Gravity γ (kN/m^3)	Cohesion c (kPa)	Angle of internal friction φ (°)	The compression modulus E_s (MPa)
0.3	20	15	20	17

pile in the code), the calculation of the horizontal allowable soil resistance h of the foundation can be divided into two cases according to the size of the transverse slope i of the foundation.

When $i \approx 0$ or can be negligible, it is calculated according to Equation (13-1).

When $0 < i \le \phi_0$, it is calculated according to Equation (13-2).

$$\begin{cases} [\sigma_H] = \dfrac{4}{\cos\varphi}[(\gamma_1 h_1 + \gamma_2 h_2)\tan\varphi + c], & (13\text{-}1) \\ [\sigma_H] = 4(\gamma_1 h_1 + \gamma_2 h_2)\dfrac{\cos^2 i\sqrt{\cos^2 i - \cos^2\phi_0}}{\cos^2\phi_0}, & (13\text{-}2) \end{cases} \tag{13}$$

where γ_1 and γ_2 are the unit weight of the soil on and below the sliding surface, respectively. h_1 is the distance between the sliding surface of the pile and the ground; h_2 is the distance between the sliding surface and the calculation point, as shown in Figure 4.

According to the actual working conditions, the soil parameters are shown in Table 1. The length of the antislide pile is 20 m, and the buried depth is 13 m. The soil of the upper and lower layers of the sliding body is loess and paleosoil, respectively, and the pile ends are embedded into bedrock. It is assumed that the homogeneous soil slope of the studied is very gentle, and $\gamma_1 = \gamma_2, \gamma_1 h_1 + \gamma_2 h_2 = \gamma H k_0$. The relationship curve between allowable soil resistance and depth in front of anchorage section pile can be calculated by Equations (11) and (13-1), and the corresponding results are shown in Figure 5(a). Figures 5(b) and 5(c), respectively, show the change results of the internal friction angle calculated according to the standard specification and the method proposed in this paper under the condition of cohesion $c = 15$ kPa; Figures 5(d) and 5(e), respectively, show the change results of the internal friction angle calculated according to the standard specification and the method proposed in this paper under the condition of internal friction angle $\varphi = 20°$.

As can be seen from Figure 5(a), the initial allowable compressive stress calculated by Equation (11) is greater than the given value in the standard specification formula, but the growth rate of critical soil resistance in the reference standard specification formula with the increase of depth is slightly greater than the calculated value in Equation (11). What is more, when the depth of soil is constant, with the increase of the internal friction angle of soil, although both formulas show nonlinear growth, the influence of soil parameter φ on the calculation formula in this paper is more and more obvious (Figures 5(b) and 5(c)). According to Figures 5(d) and 5(e), when the soil depth is constant, the critical soil resistance calculated by the formula proposed in this paper is slightly less than the allowable soil resistance calculated by the standard specification formula. However, in terms of the growth rate, the critical soil resistance calculated by the formula proposed in this paper is greatly affected by the soil strength parameter c, which shows a faster growth characteristic. It shows that the method of the standard specifications is not sensitive to the change of soil parameters and the design is conservative.

4. Finite Element Analysis

4.1. Design of Model Scheme. Midas software was used to analyze the distribution form, variation rule, and distribution characteristics of soil resistance in front of pile under horizontal load. In the operation, it is assumed that the sliding thrust of slope body is replaced by the displacement load of pile top, and the transverse slope factor is ignored. In addition, the influence of factors such as pile cross-sectional area, soil properties around pile, strength parameters, and soil heterogeneity is taken into consideration.

4.2. Establishment of the Model

4.2.1. Division of 3D Meshes and Units. According to the calculation accuracy and model size of the experimental results, 9582 elements were divided in Ansys, and then, the model was imported into Midas. It is assumed that the width of the pile is 2 m in the x direction (front and back of the pile) and 3 m in the y direction (side of the pile). The width of the model is 20 m at both sides and 30 m at the front and rear, 10 times the pile diameter. The boundary distance between the pile tip and the bottom of the model is 7 m, as shown in Figure 6(a).

The results of the model show that the calculation results do not converge and the bearing capacity of the pile is less than the empirical value when the contact surface is only set on each surface where the pile is buried. Only when the interface element is set on the rear interface and does not penetrate to the bottom of the pile, the calculated result is close to the actual one. This phenomenon can be explained as follows: the pile rotates around a certain point under the action of horizontal force, but below that point, the pile and soil are still in close contact. The setting of the contact surface in the full length of the pile-soil interface will lead to displacement distortion of soil behind the pile and mutual intrusion of units on both sides of the contact surface. Therefore, the specific setting situation is shown in Figure 6(b).

4.2.2. Material Constitutive Model and Parameters. The lateral stiffness of antislide pile embedded in the soil is much

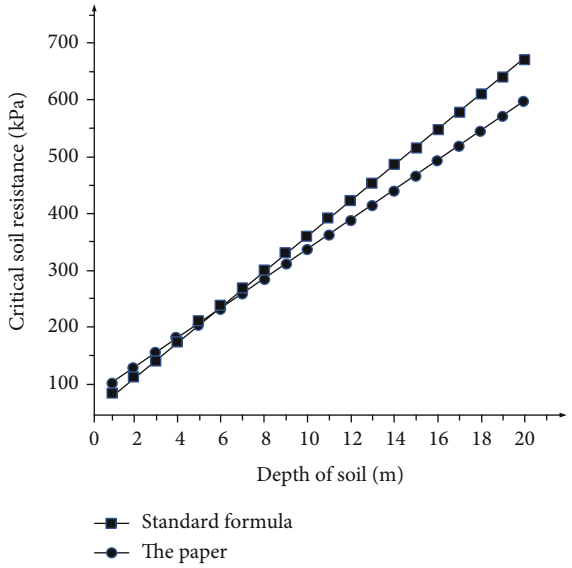

(a) Different depth

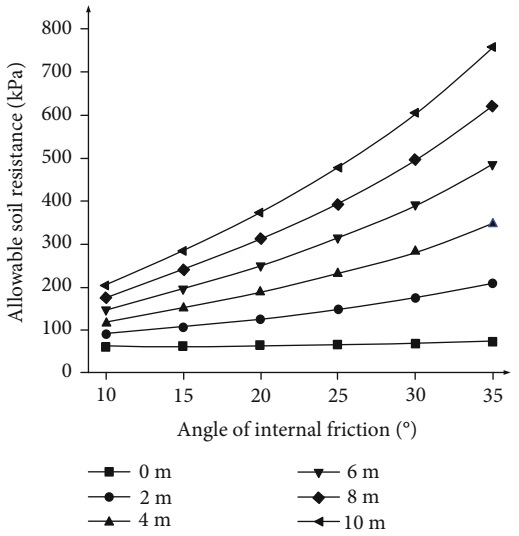

(b) Different angle of internal friction (standard specifications)

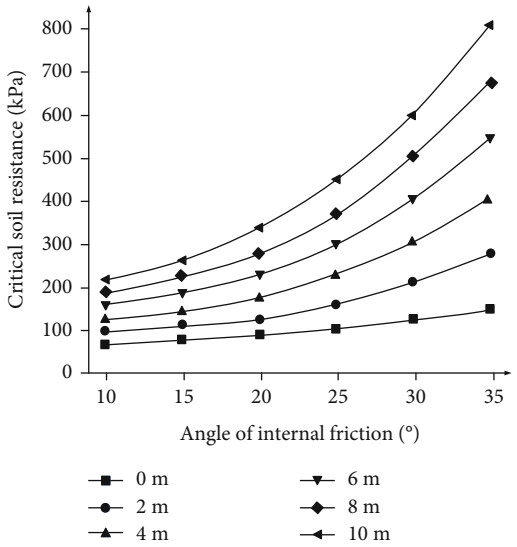

(c) Different internal friction angles (the paper)

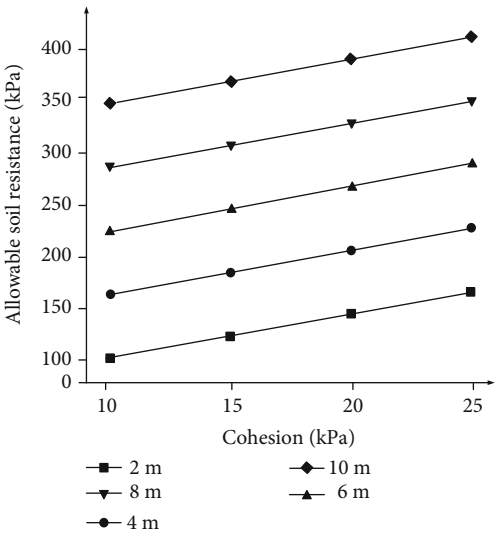

(d) Different cohesion (standard specifications)

Figure 5: Continued.

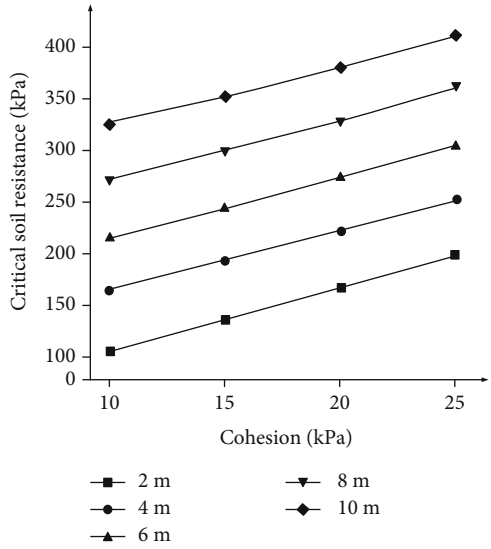

(e) Different cohesion (the paper)

Figure 5: Comparison diagram of critical soil resistance.

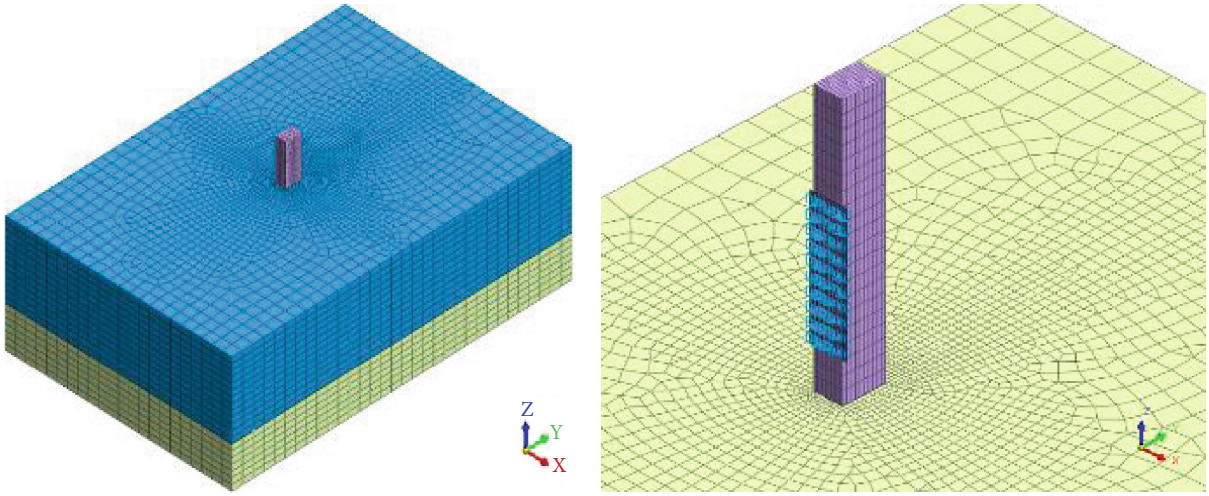

(a) (b)

Figure 6: Schematic diagram of model grid.

greater than that of the soil around the pile, and it is difficult to produce deformation under high stress. Therefore, the soil layer is regarded as an elastoplastic body, and the antislide pile is regarded as a homogeneous linear elastomer. According to the actual engineering cases, the relevant parameters of rigid pile concrete and soil are selected as shown in Table 2.

4.2.3. Boundary Conditions and External Loads. Boundary conditions adopted in the finite element model are shown in Figure 7(a). The horizontal displacement load of pile top was used to replace the acting force of sliding force on pile during the process in landslide. A rigid block with an elastic modulus of 100 GPa and an area of 2 m × 2 m was set between the horizontal displacement and the pile. The displacement of the pile top increased from 2 mm to 500 mm so that the load acted on the center of the rigid block at 1 m away from the pile top to prevent the forced displacement load from generating stress concentration on the pile top, as shown in Figure 7(b).

4.3. Results and Analysis. The shear forces at different sections of the pile were selected form the position 2 m away from the pile top (the lower edge of the rigid block) according to the equal spacing (1 m) to obtain the shear force distribution diagram of the pile under various loads, as shown in Figure 8. The model results show that the shear force at the cantilever section above the surface of the pile

Table 2: Numerical simulation of material parameters.

Soil layer	Weight γ (kN·m^{-3})	Moisture content ω (%)	Saturation (%)	Void ratio e	Cohesion c (kPa)	Angle of internal friction φ (°)	Compression modulus E_s (MPa)	Modulus of elasticity E (MPa)
Loess	19.7	23.5	75	0.93	15	14	9	—
Paleosoil	19.8	24.4	86	0.78	16	15	9	—
Concrete	25	—			—	—	—	18300
Steel	78	—			—	—	—	200000

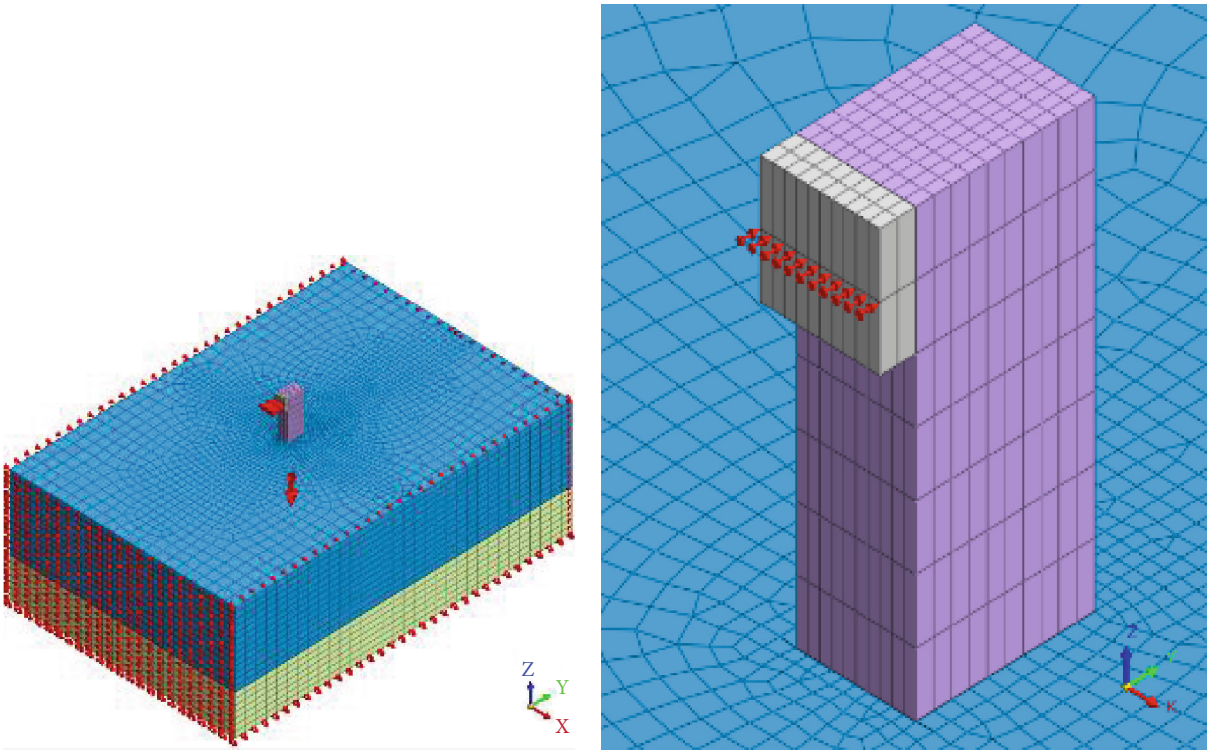

(a) Constraints on boundary displacement

(b) An enlarged view of the model loading

Figure 7: Boundary conditions and external loads.

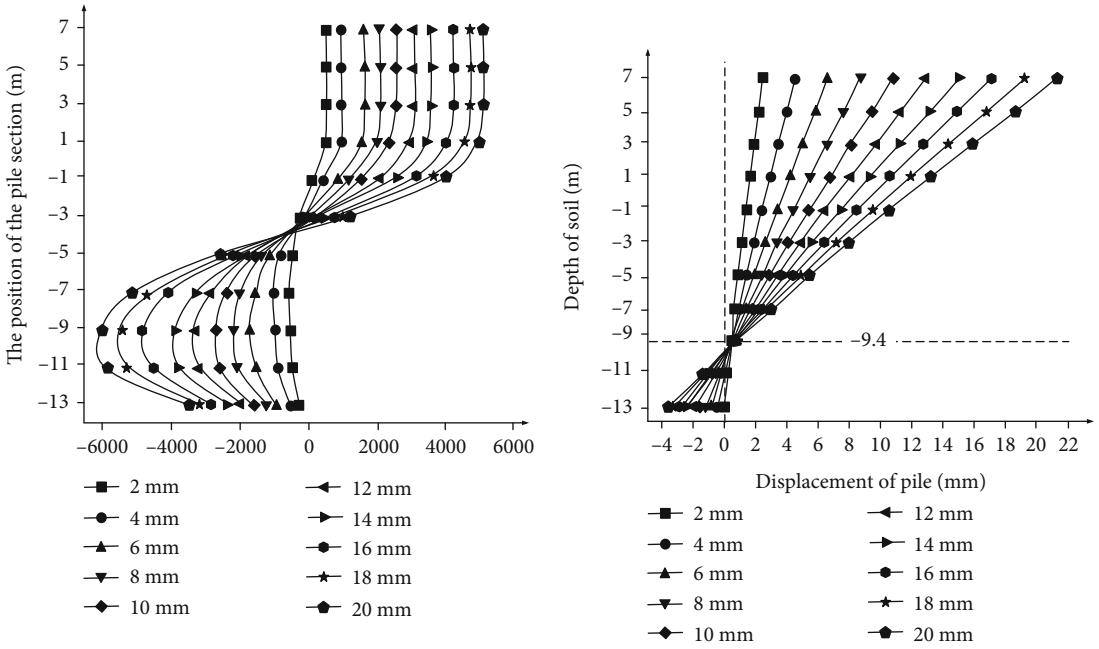

(a) Shear force of pile section

(b) The distribution of pile displacement

Figure 8: The shear and displacement distribution of pile.

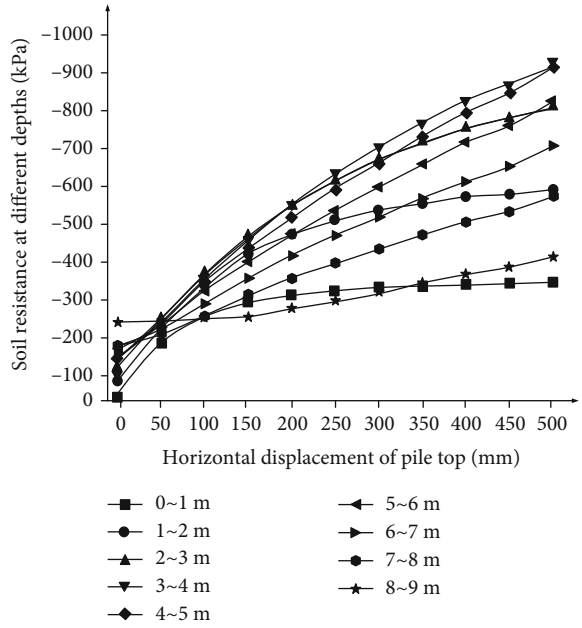

Figure 9: The growth law of soil resistance in front of the pile.

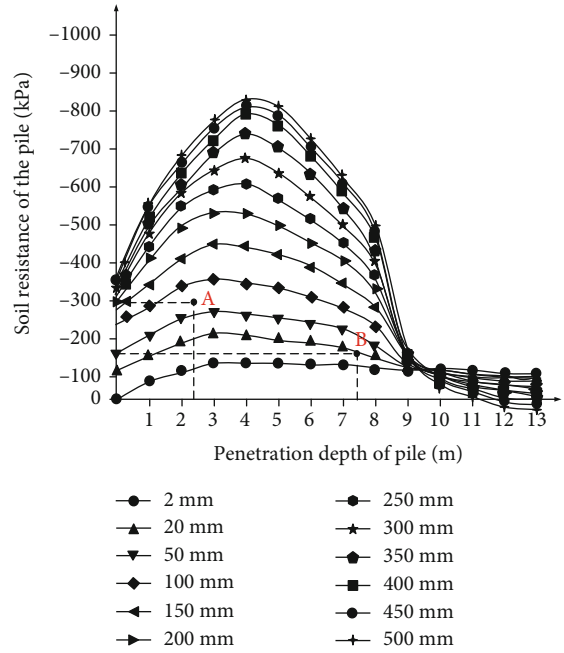

Figure 10: Soil resistance in front of pile is distributed along pile body.

remains constant, and the shear force at the pile section below the surface increases first and then decreases with the depth of the soil layer, reaching the peak point of shear stress around 9 m.

Under the horizontal load of pile top, the bearing capacity of rigid antislide pile mainly depends on soil resistance in front of pile and lateral friction resistance of pile. From Figure 8(b), the different cross-sectional location of displacement of the pile has a linear growth with the increase of soil depth, the overall distribution is "sector," in the ground below the 9.4 m for the displacement value of pile body sign change point, to the soil depth of 9.4 m from the ground displacement of pile body is positive, and the pile displacement beyond 9.4 m is negative, the pile body is turning around this point occurs.

4.3.1. The Relationship between Displacement of the Pile and Soil Resistance. The soil resistance in front of the pile at different depths is extracted, to study its variation with the horizontal displacement of the pile top, as shown in Figure 9.

The load displacement acting on the pile top is highly correlated with the soil resistance in front of pile at different depths (Figure 9). Under the condition of constant load, the soil resistance in front of pile top is positively correlated with the load displacement of pile top. When the depth of soil layer is less than 3 m, the soil yield phenomenon appears. The soil resistance in front of the pile gradually slows down with the increase of displacement load. The soil resistance in front of the pile still shows a linear growth trend, and the increase decreases gradually with the increase of soil depth when the soil depth is greater than 3 m. For example, when the soil depth is 0~1 m, 1~2 m, and 2~3 m, the pile top load displacements corresponding to soil yield are 150 mm, 300 mm, and 400 mm, respectively. One possible explanation is that the yield degree of soil in front of pile is related to the depth of soil layer. In other words, the deeper the depth of soil layer is, the more obvious the yield phenomenon of soil in front of pile is. Moreover, the horizontal self-weight stress σ_2 is proportional to the depth of soil layer, and the additional stress $\sigma_1 - \sigma_3$ of soil reaches the ultimate strength that is larger.

In order to further explore the distribution law of soil resistance in front of the pile along the pile body and the change of soil resistance in front of the pile under different loads, the distribution of soil resistance in front of the pile under different displacements is studied, and the corresponding results are shown in Figure 10.

As shown in Figure 10, the soil resistance in front of the pile basically keeps an upward trend with the increase of depth under the condition of constant load when the horizontal displacement of pile top is no more than 20 mm; the curve begins to decrease slowly as the depth exceeds 4 m (Figure 10) As mentioned above, the pile rotates roughly around 9.4 m under the horizontal displacement load of the pile top, and the horizontal displacement of the pile decreases linearly with the depth. However, the foundation coefficient of the soil beside the pile is positively proportional to the increase of soil depth. The test results show that 4 m is a turning point, the decrease of horizontal displacement above this point has less influence on soil resistance in front of the pile than that of foundation coefficient, and the increase of foundation coefficient below this point and the decrease of displacement basically cancel each other. In addition, the soil resistance in front of the pile continues to decrease significantly when the depth is greater than 4 m. As the horizontal displacement of pile top further increases, the distribution of soil resistance in front of pile becomes

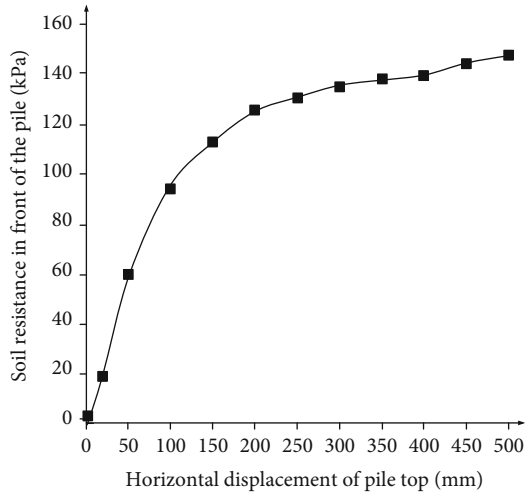

Figure 11: Resistance of soil in front of pile at 0~1 m depth.

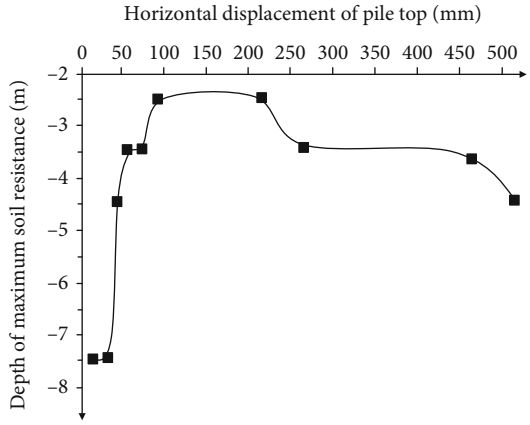

Figure 12: Position of maximum soil resistance in front of pile.

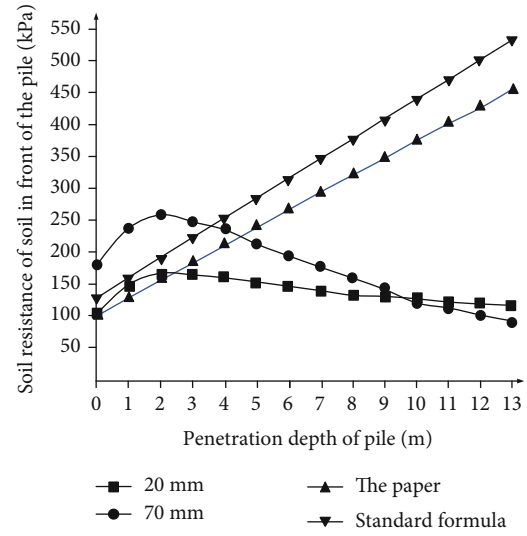

Figure 13: Comparison of theoretical and numerical results.

more and more obvious along the pile, and the difference between the maximum and minimum values increases significantly. This shows that the upper sliding soil has a strong thrust effect on the pile, resulting in obvious stress concentration of the pile top load in the soil in front of the pile. What is more, the soil resistance in front of the pile appears negative when the load is greater than 9.4 m. This is because with the increase of the depth of the bottom of the pile before the extrusion of soil under pile is small, pile body to the side of the sliding body flexure deformation occurred.

The distribution of foundation has an important relationship with the form of load, such as strip load. Accordingly, this paper takes the soil resistance at the midline section of the pile within the depth range of 0~1 m as an example, to further discuss the distribution of soil resistance in front of the pile and its variation trend with the increase of load. The variation rule of soil resistance in front of the pile under different horizontal displacements of the pile top is shown in Figure 11.

As we can see from Figure 11, with the increase of the horizontal displacement of pile top, the distribution of soil resistance in front of the pile shows obvious stress concentration, and the gap between the soil resistance on both sides in front of the pile and the soil resistance in the middle gradually increases. The soil resistance in front of the pile increases rapidly with the increase of pile top displacement load. When the pile top displacement exceeds 100 mm, the curve changes from sparse to dense, and the soil resistance in front of the pile becomes smaller under the influence of the horizontal displacement of the pile top. The process shows that the pile is subjected to more and more sliding thrust with the gradual increase of the horizontal displacement of the pile top, but the soil in front of the pile cannot provide enough resistance, and finally, the pile is damaged and the slope is unstable.

4.3.2. Ultimate Soil Resistance. According to engineering experience, when the pile side soil reaches the ultimate soil resistance, plastic flow or softening will occur. It is of great significance to explore the variation law of the ultimate soil resistance section position with the horizontal displacement of pile top for the design and the stability checking of pile foundation.

Several turning points were selected to make the curve of the maximum soil resistance position in front of the pile with the horizontal displacement of the pile top, as shown in Figure 12. When the displacement load is less than 20 mm, the maximum soil resistance position in front of the pile is about 7.5 m. Steep rise occurs and reaches a peak value in the range of 20~70 mm, indicating that the soil in front of the pile changes from elasticity to plasticity at this time and the maximum soil resistance depth is 1.88 m and continues to maintain a stable state in the range of 70~200 mm. Then, it drops slowly; it indicates that the soil in front of the pile is gradually yielding from plastic. Since there may be some differences between the grid division

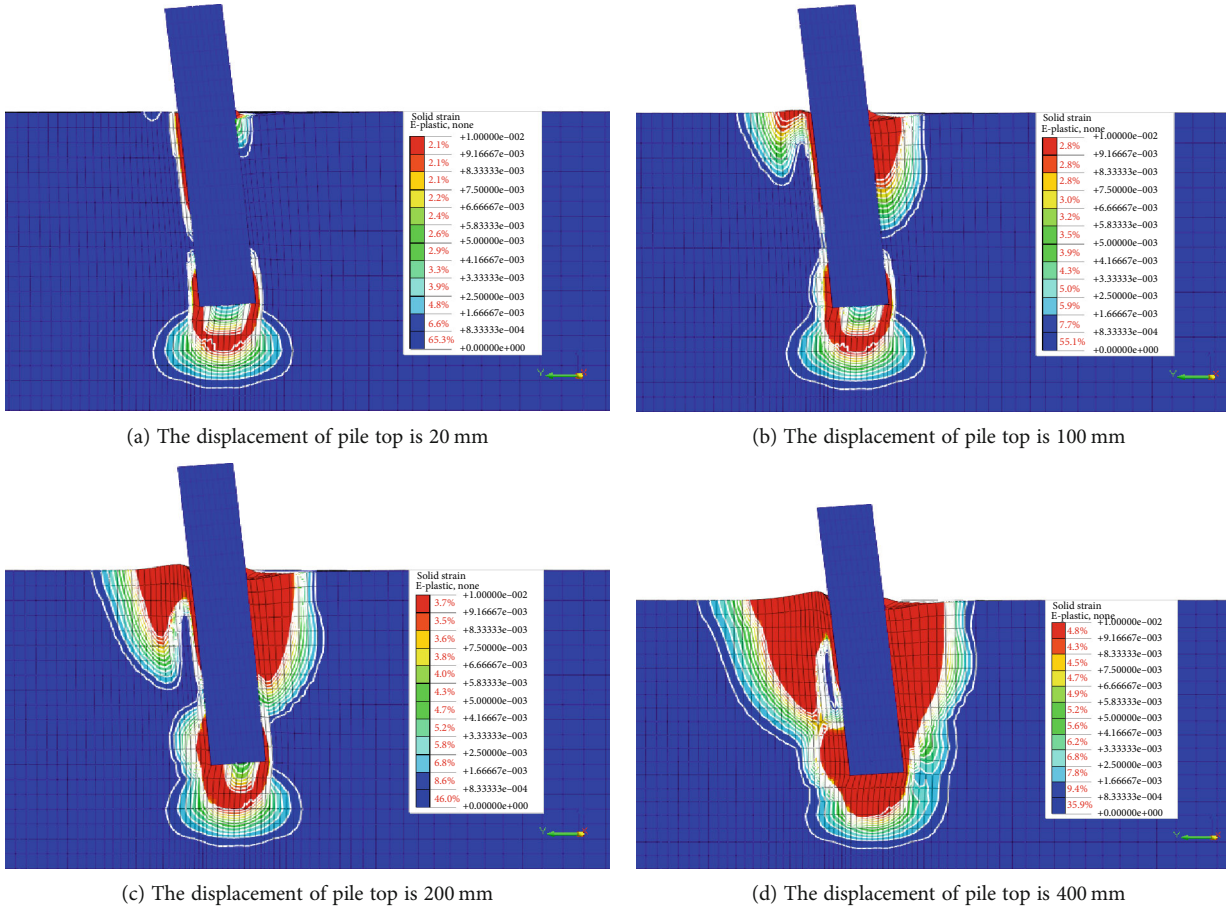

(a) The displacement of pile top is 20 mm

(b) The displacement of pile top is 100 mm

(c) The displacement of pile top is 200 mm

(d) The displacement of pile top is 400 mm

Figure 14: Plastic division layout of vertical profile of soil around pile.

Table 3: Similarity ratio of model test.

Item	Physical quantity	Relationship of similarity	Similarity ratio
Geometry	Geometric dimensioning l	C_l	1 : 10
Load	Strain	C_ε	1 : 1
	Force F	$C_F = C_\sigma C_l^2$	1 : 200
	Torque M	$C_M = C_\sigma C_l^3$	1 : 2000
Concrete	Modulus of elasticity E	C_E	1 : 2
	Poisson's ratio μ	C_μ	1 : 1
	Stress σ	$C_\sigma = C_E \cdot C_\varepsilon$	1 : 2
The soil sample of the model	Cohesion c	$C_c = C_E \cdot C_\varepsilon$	1 : 2
	Angle of internal friction φ	C_φ	1 : 1
	Modulus of compression E_s	$C_{E_s} = C_F/C_l^2$	1 : 2

and the actual stratum, the fitting curve in the figure represents the overall change of the section position of maximum soil resistance. When the horizontal displacement of pile top is 20 mm and 70 mm, correspondingly, the soil resistance at point A and point B in Figure 10 is 259.615 kN and 129.808 kN, respectively, which can be used as reference values of the ultimate soil resistance and the proximal plastic soil resistance in front of pile.

In the elastic stage, the load between pile and soil is proportional to the displacement, and the deformation and soil

Table 4: Physical and mechanical properties of the prototype soil.

Item	Loess	Paleosoil
Moisture content ω	23.5	24.4
Gravity γ	17.3	18.6
Void ratio e	0.93	0.78
Saturability s	75	86
Liquid limit I_l	31.5	30.1
Cohesion c	32	32
Angle of internal friction φ	24.6	25.3
Modulus of compression E_s	16.5	15.8

resistance decrease successively from pile top to pile tip. When the complete plastic deformation occurred in the soil before the pile, the soil around the pile that reached the horizontal ultimate resistance has yielded, and its resistance is no longer proportional to the horizontal displacement of the pile top. Moreover, the soil near the pile bottom also begins to yield, and its soil resistance basically does not change. Essentially, the process of pile instability is the process of gradual yield failure of the soil in front of the pile.

It is assumed that the shear strength parameters of soil layer in the anchorage section of antislide pile are $c = 15$ kPa and $\varphi = 20^\circ$. The soil resistance value in front of the pile corresponding to the displacement of 20 mm and 70 mm, the calculation formula in the paper, and the variation rule of soil resistance value obtained from the specification with soil depth are summarized in Figure 13.

In the process of pile rotation, the soil in front of the pile is compressed, and the soil resistance gradually decreases with the change of soil depth. In other words, the soil at different depths does not undergo plastic failure at the same time. In comparison, the results in this paper are relatively lower than the standard specification. As the previous analysis, this is because the effect of soil depth is more considered in the standard formula. The compactness and porosity of soil near the pile bottom are affected by the depth of soil layer, and it is complicated and tedious to calculate the layered soil. Therefore, the standard is simplified, and the increase of soil resistance caused by the shear strength of soil with the increase of depth is regarded as the result of the better soil properties caused by the increase of depth. The formula deduced in this paper is suitable for deep soil stratum with gentle slope.

As shown in Figure 14, vertical profiles of plastic zone distribution of soil around the pile with horizontal displacements of 20 mm, 100 mm, 200 mm, and 400 mm on the pile top are, respectively, shown. The pile body also has transverse deflection, which causes the pile tip and the pile-soil contact surface to have a large deformation. It can be seen that under the horizontal displacement of pile top, the soil around the pile produces compression deformation or even fracture failure, and the plastic zone of soil between piles interleaves and overlaps. The reason is that the stiffness of antislide pile is large and the soil behind the pile cannot provide enough lateral compressive strength [19–21]. At the same time, the soil around the pile also deforms inhomogenously, resulting in soil arching effect. When the load behind the pile approaches the limit value, the range of plastic zone in the soil expands, the pile and soil mutual dislocation occurs, and the relative displacement increases sharply. The plastic zone develops from the back side of the pile to the front side of the pile, and until the plastic zone is connected, the soil arch is destroyed, the antislide pile loses its retaining function, and the soil is destroyed by extrusion [22]. In this process, the pile tends to be pulled out upward, and the destruction process of soil arch just reflects the development law of plastic zone.

5. Indoor Model Test

5.1. Similarity Ratio of Model Test. In order to simulate the failure mode and failure mechanism of rigid antislide pile under horizontal load in reality and to compare with the simulation results and verify its accuracy, laboratory model test is now carried out. The relationship of similarity ratio is shown in Table 3, and the material parameters of model soil and prototype soil are selected according to Tables 4 and 5.

5.2. Test Elements and Soil Layer Setup in Model Test. Horizontal load is applied by MTS brake in the test, the maximum is 50 kN, and the maximum horizontal displacement that can be applied is 260 mm. The displacement increment is set as 2 mm before the test. The brake is loaded automatically during the test. A square steel plate gasket of 300 mm × 300 mm is set at the contact point between the brake and the pile top, and the operating point is about 20 cm from the pile top.

First, the model box is processed. Channel steel frame and wooden baffle are used around the model box for retaining protection. According to Figure 15(a), the model pile was put in place, and then, the soil sample of the model was layered and tamped. At each predetermined filling height, the test components were laid out according to Figure 15(b). The horizontal displacement of pile top takes 10 mm as the first level and is loaded until the maximum displacement. The loading time interval is 15 min. Finally, the data are read and recorded. Figure 16 is the layout and loading diagram of the model box.

5.3. Characteristics of Soil Resistance in front of Rigid Antislide Pile. As shown in Figure 17, take the earth pressure cell with a buried depth of 0.55 m as an example. The two curves of numerical simulation and model test almost have the same change rule. The inflection point of the numerical simulation curve is about 14 mm, and the critical point is about 34 mm. The curve of numerical simulation appears a turning point at about 14 mm and reaches a critical point at about 34 mm. Firstly, the horizontal load of pile top has a linear relationship with the horizontal displacement of pile top, and applying a large force on pile top can only cause a small displacement. In the elastoplastic stage, a small load on the pile top can make the pile produce a large displacement, and the increased displacement is about 26.5% of that

Table 5: Model material parameters.

Material	Moisture content ω (%)	Gravity γ (kN·m^{-3})	Cohesion$c$ (kPa)	Angle of internal friction φ (°)	Modulus of compression E_s (MPa)	Modulus of elasticity E (MPa)
Loess	19.10	19.70	15.0	5.60	5.30	
Paleosoil	17.30	19.80	8.50	5.80	5.98	
C15 concrete		25				18300
HRB400 steel		78				200000

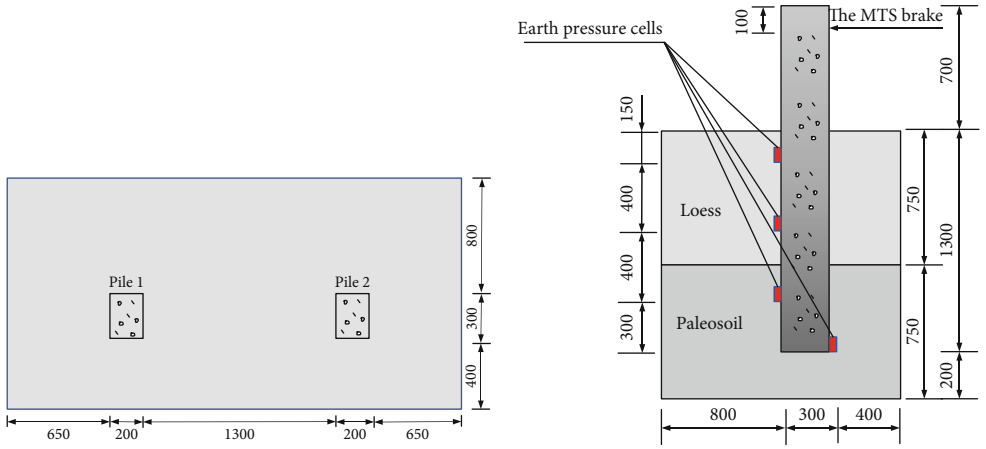

(a) The arrangement of piles (b) Layout of test components

Figure 15: Model and test component layout (unit: mm).

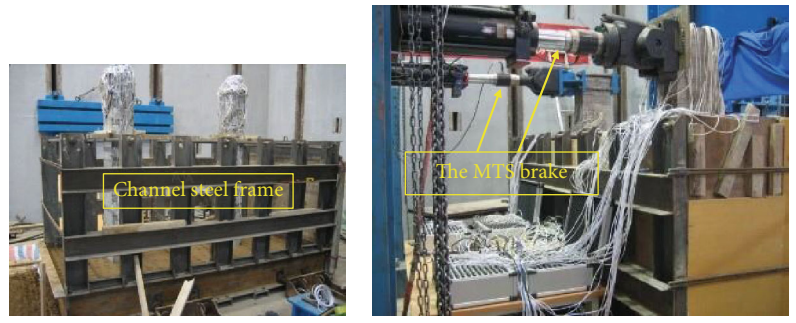

(a) (b)

Figure 16: Schematic diagram of layout and loading of model box.

in the first stage. When the soil around the pile becomes plastic completely, the displacement reduction is even lower than the previous stage, and the displacement increase is about 22.3% of that in the first stage.

Selecting the equivalent spacing of 0.05 in Midas, we can draw the contour map of plastic strain zone of soil in front of pile under various displacements on pile top which is made in Figure 18. As can be seen from the figure, the larger the horizontal displacement of pile top, the plastic zone of soil behind pile manifests the characteristics of obvious development along a certain direction. At the beginning, the plastic zone develops towards the front and bottom of pile at the same speed. And the border of piles and soil are angled 45°, roughly when the load reached 32 mm plastic zone obviously to the lower range of deeper development, combined with Figure 17 found that due to the numerical calculation at the beginning of the displacement of pile top level reaches 68 mm not convergence, the maximum range of the plastic zone does not appear in the pile soil contact surface or maximize lateral displacement of the pile body, but deep under the ground [23, 24].

As shown in Figure 19, the pile inclines under the strong thrust of the sliding body, compresses the soil in front of the pile, and makes the soil reach the ultimate resistance and

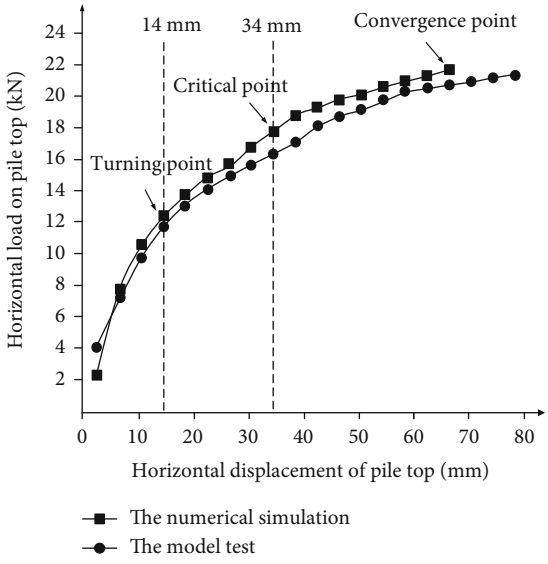

Figure 17: Displacement-load relation diagram of pile top.

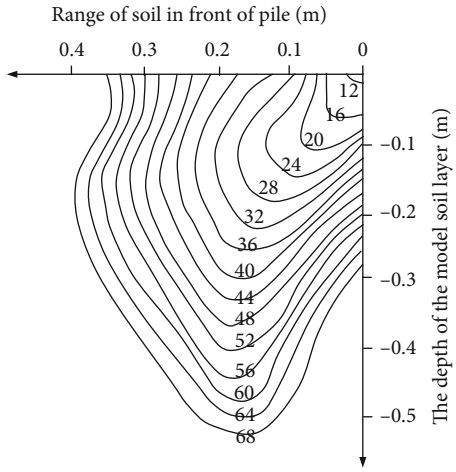

Figure 18: Isolate map of plastic zone in front of pile under different loads.

Figure 19: Fracturing damage of soil in front of pile.

causes obvious fracturing failure. The soil behind the pile is separated from the pile. With the increase of pile penetration depth, the model test data are basically smaller than the results of the finite element analysis. This is because the cross-sectional stress selected for the model test is relatively low, and the soil resistance in front of the pile is not uniformly distributed on the pile compression surface, so the simulation results select the average cross-sectional stress. Shallow middle soil is basic to yield, located close to neutral point to 0.95 m in soil pile lateral soil resistance is about 0, displacement of the pile side soil resistance of positive and negative change point up and down is relatively close, the pile lateral soil resistance in the nearer distance from the surface of the soil to more fully, displacement of pile lateral soil resistance and the location of the positive and negative points of variability, the farther the distance that point displacement is larger. Therefore, the pile side soil resistance is greater [25].

6. Conclusion

(1) Through theoretical analysis, the theoretical formula of the proximal plastic soil resistance in front of pile with the change of soil depth is obtained and compared with the code. The results show that the standard is not sensitive to the change of soil parameters and the design is conservative. The influence of soil parameters on soil resistance in front of pile should be considered in subsequent engineering construction

(2) Values of soil resistance 129.808 kN and 259.615 kN can be used as reference values of proximal plastic soil resistance and ultimate soil resistance in front of rigid antislide pile, respectively. In essence, the failure process of soil arch around the pile reflects the development law of plastic zone below the buried depth of pile. When the maximum soil resistance section reaches the peak value, the horizontal bearing capacity of the pile is taken as the limit value of the horizontal bearing capacity of the rigid antislide pile

(3) The results of laboratory model test showed that the plastic zone below the depth of pile expands in a certain direction. At the beginning, the plastic zone develops to the front and bottom of the pile at the same speed, at an angle of 45° with the direction of gravity. When the displacement reaches 34 mm, the plastic zone develops to the lower depth obviously. The greater the horizontal displacement of pile top is, the greater the relative displacement between pile and soil will be. When the soil resistance in front of pile reaches the limit value, the relative displacement between pile and soil will increase sharply until the plastic zone is connected, the retaining effect of pile will fail, and the slope will be unstable

Data Availability

The test data used to support the findings of this study are included within the article. Readers can obtain data supporting the research results from the test data table in the paper.

Conflicts of Interest

The authors declare no conflict of interest.

Authors' Contributions

Zhenyu Song formulated the research ideas of the paper and collected and summarized all experimental data; Yaunyaun Kong checked the article and put forward some crucial suggestions; Siqi Wang assisted to complete numerical simulation, checked the article, and put forward some crucial suggestions; Weifeng Zhao checked the article and put forward some crucial suggestions; Lu Chen assisted to complete numerical simulation and helped translate the paper; Kai Feng extracted data of the model test and provided guidance for ideas during the experiment.

Acknowledgments

I would like to thank all the members of the research group for their concern and help, especially my mentor, Professor Kong Yuanyuan. I would like to thank my workmates for their care and encouragement in my study and life. Thank you for your company in the course of the experiment; I move forward bravely in the face of various setbacks.

References

[1] S. H. E. N. Zhujiang, "Sliding resistance and ultimate design of pile," *Chinese Journal of Geotechnical Engineering*, vol. 1, pp. 51–56, 1992.

[2] R. K. Rowe, "Pile foundation analysis and design: book review," *NRC Research Press Ottawa, Canada*, vol. 18, no. 3, pp. 472-473, 1981.

[3] S. S. Rajashree and T. G. Sitharam, "Nonlinear finite-element modeling of batter piles under lateral load," *Journal of Geotechnical and Geoenvironmental Engineering*, vol. 127, no. 7, pp. 604–612, 2001.

[4] X. I. A. O. Shiguo, "Analysis method and engineering application of H-type composite anti-slide pile in slope treatment," *Rock and Soil Mechanics*, vol. 31, no. 7, pp. 2146–2152, 2010.

[5] Z. H. A. N. G. Lei, G. O. N. G. Xiaonan, and Y. U. Jianlin, "Study on nonlinear foundation reaction method for horizontal load calculation of single pile," *Chinese Journal of Geotechnical Engineering*, vol. 33, no. 2, p. 309, 2011.

[6] Yokoyama, *Calculation Method and Example of Pile Structure*, China Railway Publishing House, 1984.

[7] L. K. Ginzburg and V. I. Ischchenko, "Computation of an anchored antislide pile design," *Soil Mechanics and Foundation Engineering*, vol. 19, no. 5, 1982.

[8] H. Matlock, "Correlation for design of laterally loaded piles in soft clay," in *Offshore technology conference*, OnePetro, 1970.

[9] M. W. M. J. M. O'neill, "An evaluation of p-y relationships in sand," *A Report to American Petroleum Institute*, University of Houston, Houston, 1983.

[10] G. A. O. Ming, C. H. E. N. Jinzhen, Z. H. E. N. G. Guofang, and F.A.N.G. Huolan, "Study on pile performance under lateral static, dynamic and cyclic loads and suggested formula of P-Y curve," *Ocean Engineering*, vol. 3, pp. 36–46, 1988.

[11] W. A. N. G. Teng, D. O. N. G. Sheng, and F. E. N. G. Xiuli, "Influence of soil parameters on horizontal response of pile foundation," *Rock and Soil Mechanics*, vol. 25, S1, pp. 71–74, 2004.

[12] W. Chenglei, W. Jianhua, and F. Shilun, "Analysis of p-y relationship of pile-soil interaction under soil liquefaction," *Chinese Journal of Geotechnical Engineering*, vol. 29, no. 10, pp. 1500–1505, 2007.

[13] L. I. Yurun, "Study on correction calculation method of p-y curve of pile-liquefied soil interaction," *Journal of Geotechnical Engineering*, vol. 31, no. 4, pp. 595–599, 2009.

[14] Z. H. A. N. G. Jianhua, X. I. E. Qiang, and Z. H. A. N. G. Zhaoxiu, "Soil arching effect and its numerical simulation of anti-slide pile structure," *Chinese Journal of Rock Mechanics and Engineering*, vol. 4, pp. 699–703, 2004.

[15] X. I. N. Jianping, Z. H. E. N. G. Yingren, and T. A. N. G. Xiaosong, "Failure mechanism of micro-anti-slide pile based on elastic-plastic model," *Chinese Journal of Rock Mechanics and Engineering*, vol. 33, no. A02, pp. 4113–4121, 2014.

[16] J. I. A. N. G. Xin, L. I. U. Jinnan, H. U. A. N. G. Mingxing, and Y.-j. Qiu, "Numerical simulation of reinforcement of embankment on soft slope foundation by anti-slide piles," *Rock and Soil Mechanics*, vol. 33, no. 4, pp. 1261–1267, 2012.

[17] J. I. N. Qing, C. U. I. Xinzhuang, and L. I. U. Zhengyin, "Numerical analysis of lateral bearing capacity of rigid piles," *Rock and Soil Mechanics*, vol. 27, S2, pp. 814–817, 2006.

[18] TB 10025-2001, *Code for Design of Railway Subgrade Support Structure*, People's Communications Press, Beijing, 2001.

[19] C. M. MARTIN and M. F. RANDOLPH, "Upper-bound analysis of lateral pile capacity in cohesive soil," *Geotechnique*, vol. 55, no. 2, 2006.

[20] S. Hassiotis, J. L. Chameau, and M. Gunaratne, "Design method for stabilization of slopes with piles," *Journal of Geotechnical and Geoenvironmental Engneering*, vol. 123, no. 4, pp. 314–322, 1997.

[21] L. V. Qing, S. U. N. Hongyue, and S. H. A. N. G. Yuequan, "Mechanism and development of soil arching effect behind anti-slide pile," *Journal of Hydraulic Engineering*, vol. 41, no. 4, pp. 471–476, 2010.

[22] Z. H. E. N. G. Yingren, C. H. E. N. Zuyu, and W. A. N. G. Gongxian, *Engineering Treatment of Slope & Landslide*, China Communications Press, Beijing, 2007.

[23] Z. H. E. N. G. Junjie, L. V. Siqi, and C. A. O. Wenzhao, "Numerical simulation analysis of force and deformation characteristics of rigid-flexible composite anti-slide pile [J]," *Journal of Huazhong University of Science and Technology (Natural Science Edition)*, vol. 45, no. 4, pp. 39–44, 2017.

[24] Z. H. A. N. G. Xudong, Z. H. A. I. Encheng, W. U. Yajun, S. U. N. De'an, and L. U. Yitian, "Theoretical and numerical analyses on hydro-thermal-salt-mechanical interaction of unsaturated salinized soil subjected to typical unidirectional freezing process," *International Journal of Geomechanics*, vol. 21, no. 7, 2021.

[25] Z. H. A. N. G. Weimin, G. U. Xingwen, R. E. N. Guofeng, and W. U. Yingli, "Research on pile-soil interaction mechanism and ultimate resistance to sliding force of rigid anti-slide pile," *Civil engineering journal*, vol. 50, no. 10, pp. 82–90, 2017.